# Comparative Analysis of Boost and Quasi-Z-Source Converters as Maximum Power Point Trackers for PV Panel Integrated Converters

Janis Zakis, Ivars Rankis, Leonids Ribickis
Institute of Industrial Electronics and Electrical Engineering
Riga Technical University
Riga, Latvia
janis.zakis@ieee.org

***Abstract*—This paper analyzes two maximum power point tracking (MPPT) converter topologies that are part of an interface converter for the integration of photovoltaics (PV) in the grid. Two different MPPT converter topologies (boost converter and quasi-Z-Source (qZS) converter) were selected and compared. Theoretical comparison includes an analysis of regulations for obtaining continuous source current and comparison of necessary parameters of the reactive elements of the systems.**

**270 W experimental prototypes of both converters were built and experimentally compared. Theoretical and experimental efficiency estimation is proposed and discussed. Also, the losses in diodes and MOSFETS are evaluated taking into account technical data from datasheets**

***Keywords*—DC-DC power converters, boost converter, quasi-Z-source, photovoltaic system**

## I. Introduction

Distributed generation systems that use renewable energy have great potential to increase the grid potential. Photovoltaic (PV) technology that provides renewable energy is the most popular distributed energy source with zero emissions.

PV cells have nonlinear *U-I* characteristics. The output voltage and power change according to the temperature and irradiation. Fig. 1 shows the *U-I* characteristics of the selected PV stack (Saana 245-255 TP3 MBW) [1] that is accepted as a voltage source.

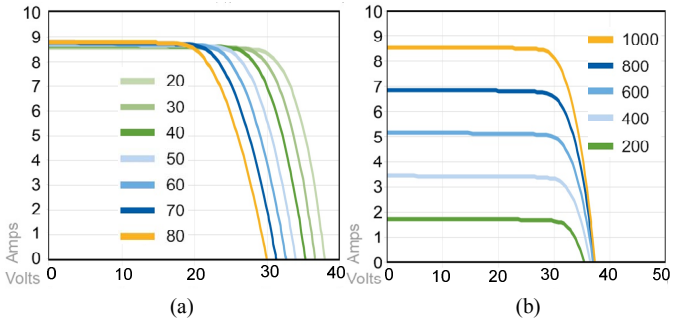


Fig. 1. *U-I* characteristics of the PV stack Saana 245-255 TP3 MBW: a) voltage/current dependence on the temperature (°C); b) voltage/current dependence on the irradiation (W/m2).

Fig. 1*a* shows the *U-I* characteristics of the cell at constant irradiation (1kW/m2) and varying temperature (°C). It can be seen that maximum power could be obtained only at the lowest cell temperature. Fig. 1*b* shows the *U-I* characteristics of the cell at constant temperature (25°C) and varying irradiation (W/m2). According to the PV stack Saana 245-255 TP3 MBW data sheet, the maximum power point MPP (255 W) is at current 8.33 A and voltage 30.6 V. To keep the operation at the maximum power point independent of the temperature and irradiation, the maximum power point tracker (MPPT) converter should be used.

Fig. 2 presents the general block diagram of the PV interface DC-DC converter. Selection of the MPPT converter topology and optimization of the parameters is essential due to high current and low voltage at the output of the PV cell.

This paper presents a comparative evaluation of a classical boost converter [2] and a quasi-Z-source (qZS) converter [3]-[6] as possible MPPT converter topologies. The second part of the PV interface converter that includes a voltage source inverter (VSI), a step-up isolation transformer and a rectifier is not discussed in this paper.

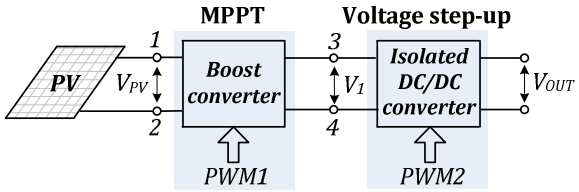


Fig. 2. General block diagram of an interface converter for a PV system.

## II. Comparative Analysis of a Boost Converter and aQuasi-Z-Source Converter

Both of the DC-DC converters (boost and qZS) can be used for voltage step-up but it is reasonable to compare their parameters and performance. A boundary case between the continuous conduction mode (CCM) and the discontinuous conduction mode (DCM) of the input current was selected as the theoretical comparison point for parameter selection of the inductors. Fig. 3 shows the equivalent circuits used for our analytical study and comparison.

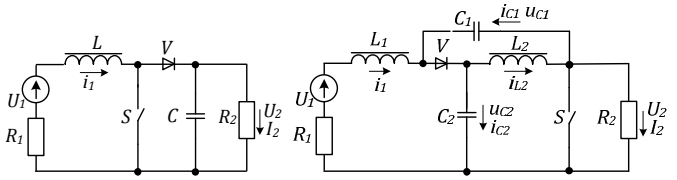


Fig. 3. Equivalent circuits of the proposed MPPT converters: a) boost converter, b) qZS converter.

### A. Boost Converter

Both the CCM and the DCM of the input current can be achieved in the classical boost converter shown in Fig. 3*a* [2]. The boundary between the CCM and DCM is revealed when the magnitude $I_{1m}$ of the triangular ripple of the input current $i_1$ is twice higher than the average value of the same current $I_{1a}$.

Accepting that the shape of the current $i_1$ ripple is triangular at the boundary case, the average value of the switch current is $I_{Sa}=0.5I_{1m}D$, where $D$ is the duty cycle of the switch but the averaged current of the diode $V$ and the load are $U_2/R_2$. An averaged current of the source in the boundary and the DCM cases is

$$I_{1a} = 0.5I_{1m}D + \frac{U_2}{R_2}. \tag{1}$$

From the balance of an input and output power it follows that $U_1 I_{1a} = \frac{U_2^2}{R_2}$ and taking into account that $I_{1m} = \frac{U_1 DT}{L}$, where $T$ is the switching cycle of the switch, we obtain

$$U_2^2 - U_2 U_1 - \frac{U_1^2 D^2 T R_2}{2L} = 0. \tag{2}$$

The load voltage in the DCM and the boundary case can be expressed as

$$U_{2b,DCM} = 0.5U_1\left(1+\sqrt{1+\frac{2R_2D^2}{Lf}}\right), \tag{3}$$

where $f$ is the switching frequency.

At the end of the discontinuous current case when $U_1=U_2(1-D_b)$, where $D_b$ is the duty cycle for the boundary case, we obtain the relation

$$\frac{2Lf}{R_2} = D_b - 2D_b^2 + D_b^3, \tag{4}$$

that allows us to find the parameters for the boundary operation case.

Fig. 4 presents the dependence curve of $2Lf/R_2=f(D_b)$. The extreme of this curve is at $D_{bm}=0.333$ when the value of the parameters $2Lf/R_2$ relation is 0.148. It means that the inductance changes of the storage coil for the continuous supply current in the whole range of $D$ have to be larger than $0.148R_2/2f$. For instance, if $R_2=50\Omega$ and $f=20$ kHz, then $L>185\mu$H.

When the converter operates in the CCM, the main expressions relative to $U_1$ or $U_1/R_2$ describing the processes are as follows (see Fig. 4):

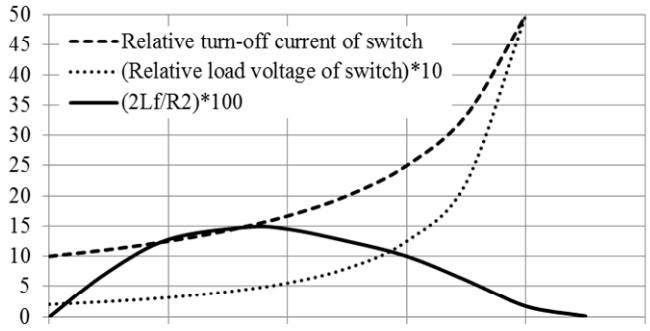


Fig. 4. General parameter characterizing the BOOST topology performance depending on the boundary duty cycle ($D_b$): $2Lf/R_2=f(D_b)$; $I^*_{SCCM}=f(D_b)$ $U^*_{2CCM}=f(D_b)$.

$$U^*_{2CCM} = \frac{1}{1-D_{CCM}};\ I^*_{1CCM} = P^*_2 = \frac{U_2^2 R_2}{R_2 U_1^2} = \frac{1}{(1-D_{CCM})^2}, \tag{5}$$

but the ripple range of the source current is

$$\Delta I^*_{1CCM} = \frac{D_{CCM} R_2}{Lf}, \tag{6}$$

i.e., the turn-off current of the switch can be expressed as

$$I^*_{SmCCM} = \frac{1}{(1-D_{CCM})^2} + \frac{D_{CCM} R_2}{2Lf}. \tag{7}$$

The storage capacitor of the load $C$ is a bulky element regarding to the maximum output voltage and must have large capacity that provides small load voltage ripple. In the calculation of the volume of the capacitor, the capacitor is discharged during the interval $D_{CCM}/f$ by the influence of the load current, i.e. its efficiency indicator is

$$\Delta U_c C = \frac{I_{ld} D_{CCM}}{f}. \tag{8}$$

### B. qZS Converter

The voltage step-up DC-DC converter with the qZS presented in Fig. 3*b* [3][4] comprises two capacitors ($C_1$ and $C_2$), two inductors ($L_1$ and $L_2$), and a diode $V_1$. When the switch $S$ is turned on, two parallel current circuits are operating - one from the DC source through the inductor $L_1$ and capacitor $C_1$, the other from the capacitor $C_2$ and inductor $L_2$. Summative current of those circuits flows through the switch $S$.

The basic expressions that characterize the continuous source current operation mode are as follows:

$$U^*_{2CCM} = \frac{1-D_{CCM}}{1-2D_{CCM}};\ I^*_{1CCM} = P^*_{2(qZ)} = \frac{1-D_{CCM}}{(1-2D_{CCM})^2},$$

$$U^*_{C2,CCM} = \frac{D_{CCM}}{1-2D_{CCM}};\ U^*_{C1,CCM} = \frac{1-D_{CCM}}{1-2D_{CCM}}, \tag{9}$$

$$\Delta I^*_{1,CCM} = \frac{D_{CCM}(1-D_{CCM})R_2}{L_1 f(1-2D_{CCM})};\ \Delta I^*_{2CCM} = \frac{D_{CCM}(1-D_{CCM})R_2}{L_2 f(1-2D_{CCM})}$$

For the same load voltage in the qZ case, the duty cycle is two times smaller compared to an ordinary boost converter, i.e. $D_{CCMqZ}$=0.5$D_{CCMB}$ .

Half of the magnitude of the input current $i_1$ in the boundary case between the CCM and the DCM is equal to the averaged current of the DC source and can be calculated as

$$I_{1mb} = \frac{U_1 D_b (1 - D_b)}{L_1 f (1 - 2D_b)} \quad . \tag{10}$$

The boundary case duty cycle can be bound with the parameters of the scheme as

$$2D_{b(qZ)}^3 - 3D_{b(qZ)}^2 + D_{b(qZ)} = \frac{2L_1 f}{R_2} \quad , \tag{11}$$

where 0<$D_{b(qZ)}$<0.5. The extreme of the expression is at $D_{bm\ (qZ)}$ =0.211 when the value of the parameter's relation is 0.0962. Fig. 5 presents the dependence curve $2L_1f/R_2$=$f(D_{b(qZ)})$. Above this relation's value the curve will be in the CCM in the whole range of the duty cycle accessible for the scheme.

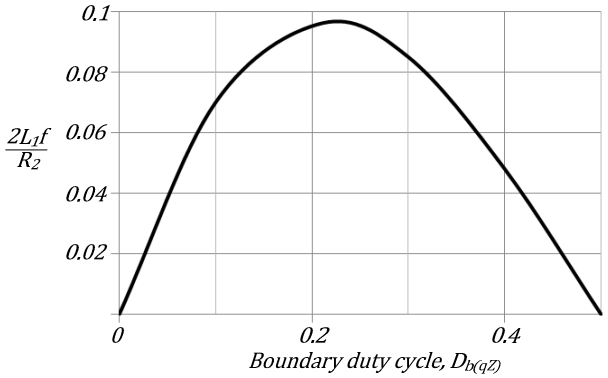


Fig. 5. Dependence of the parameter relation $2L_1f/R_2$ on the boundary duty ratio.

It means that the inductance changes of the storage inductors for the continuous supply current in the whole range of $D$ have to be larger than $0.0962R_2/2f$. For instance, if $R_2$=50 Ω and $f$=20 kHz, then $L_1$=$L_2$>120 μH.

The turn-off current of the switch $S$ can be expressed as

$$I^*_{smCCM} = \frac{2(1 - D_{CCM})}{(1 - 2D_{CCm})^2} + \frac{D_{CCM}(1 - D_{CCM})R_2}{L_1 f (1 - 2D_{CCM})} . \tag{12}$$

### C. *Comparison of Performance Parameters of Both Converters*

Both of the systems discussed have to be compared for equal values of supply and load voltages, switching frequencies and load resistance.

One of the essential parameters of the compared systems is the summary inductance of the inductors. At equal relative supply current ripple, the summary inductance of both of the inductors in the qZS converter regarding to the inductance of inductors for the boost converter is

$$\frac{2L_1}{L} = \frac{1 - 0.5D_{CCMB}}{1 - D_{CCMB}} . \tag{13}$$

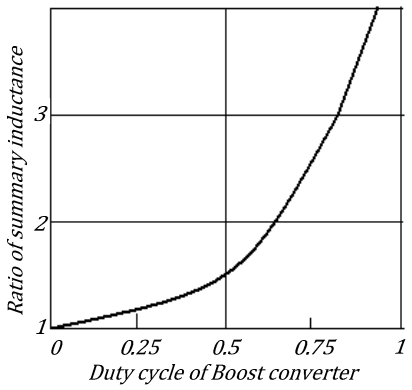


Fig. 6. Ratio of the summary inductance of inductors for qZ and boost converters depending on the duty cycle of the boost converter.

As it can be seen from Fig. 6, the relation is growing at the duty cycle value rising. If in the boost converter $D_{CCMB}$=0.8 is accepted (in the qZS converter $D_{CCMqZ}$=0.4), then the relation reaches the meaning 3, i.e. the size of inductors in the qZS converter has to be three times larger than in the ordinary boost converter.

Turn-off current of the transistor switch is another indicator characterizing converter properties. The relation of the turn-off currents for both of the discussed systems using (12) and (7) is exactly 2, i.e. the turn-off current for the transistor switch in the qZ converter is twice larger than in the ordinary boost converter, which raises extra problems twith the realization of the switch.

Fig. 7 shows experimentally obtained characteristics of the source current ripple and the turn-off current of switches $S$ at supply voltages from 15-35 V and output voltage 40 V.

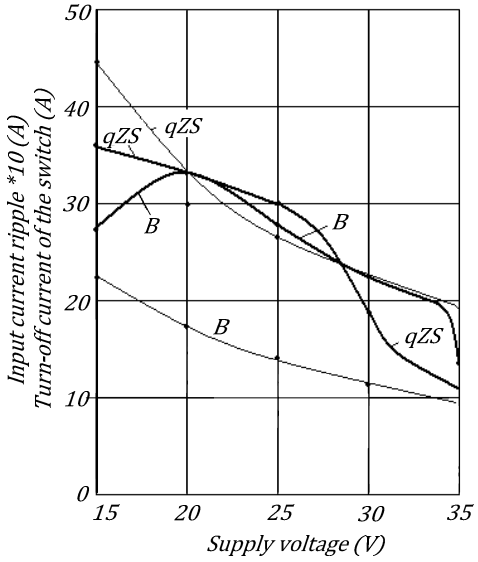


Fig. 7. Input current ripple of the discussed converters (bold line) and turn-off current of the switch (thin line) at different input voltages for both converters.

As it can be seen, the turn-off current of the transistor switch for the whole range of examined supply voltages is almost twice larger in the qZS converter compared to the boost converter. Input current ripple of both converters is almost equal and it decreases at the rise of the supply voltage.

## III. Power Loss Analysis in Semiconductors

To increase the efficiency of a PV interface converter, it is essential to pay serious attention to the MPPT part (Fig. 2). The main components that create major active power losses and reduce the efficiency in both of the discussed converters are semiconductors (switches and diodes). Our analysis of losses in the semiconductors is presented below.

### A. Power Loss Analysis in MOSFETs

Power loss calculations in the MOSFET using data sheet parameters are based on the methodology in [7]. Conduction losses in the power MOSFET can be calculated using a MOSFET approximation with the drain-source on-state resistance ($R_{DS(on)}$).

Integration of the instantaneous power losses over the switching period gives an average value of the MOSFET conduction losses:

$$P_{CM} = \frac{1}{T_{SW}} \int_0^{T_{SW}} (R_{DS(on)} \cdot i_D^2(t))dt = R_{DS(on)} \cdot I_{Drms}^2, \quad (14)$$

where $I_{Drms}$ is the rms value of the MOSFET on-state current.

Another type of losses that characterize transistor losses is the switching losses that consist of turn-on and turn-off energy losses. The worst case turn-on energy losses in the MOSFET ($E_{onM}$) can be calculated as the sum of switch-on energy and switch-on energy caused by the reverse recovery of the free-wheeling diode. In our experiments the free-wheeling diode is not employed, therefore its losses are neglected. The switch-on energy losses of the MOSFET can be obtained as

$$E_{on} = \int_0^{tri+tfu} u_{DS}(t) \cdot i_D dt = U_{DD} \cdot I_{Don} \cdot \frac{tri + tfu}{2} + Q_{rr} \cdot U_{DD}, \quad (15)$$

where

$U_{DD}$ – DC-link voltage
$I_{Don}$ – drain current at the beginning of pulse
$I_{Doff}$ – drain current at the end of pulse
*tri* – current rise time
*tfu* – voltage fall time
$Q_{rr}$ – reverse recovery charge

The switch-off energy losses in the MOSFET can be calculated as

$$E_{offM} = \int_0^{tru+tfi} u_{DS}(t) \cdot i_D(t) = U_{DD} \cdot I_{Doff} \cdot \frac{tru + tfi}{2}, \quad (16)$$

where

$I_{Doff}$ – drain current at the end of pulse
*tfi* – current fall time (from data sheet)
*tru* – voltage rise time

The total switching losses in the MOSFET are the product of switching energies and switching frequency ($f_{sw}$):

$$P_{sw} = (E_{on} + E_{off}) \cdot f_{sw} \quad (17)$$

### B. Power Losses in the qZS-Network Diode

Power losses in a diode consist of conduction losses, reverse recovery losses and reverse leakage losses. Since the Schottky diode is used in our case, the reverse recovery losses can be neglected.

Conduction losses of the diode can be calculated as

$$\Delta P_{cond} = U_{FVD} \cdot I_{rms}. \quad (18)$$

The reverse leakage losses can be found as

$$\Delta P_{cond} = I_r \cdot U_{diode}(1 - D_{diode}), \quad (19)$$

where $I_r$ is the reverse leakage current that can be found in the component data sheet.

### C. Justification of Theoretical Power Losses in Semiconductors

Based on the calculation methodology presented above, the power losses in switches *S* and diodes *V* of both converters are summarized in TABLE I.

TABLE I. Power Losses (*W*) in Semicondictors

| Converter Type | Boost | | qZS | |
|---|---|---|---|---|
| Device / Op. point | ***Switch*** | ***Diode*** | ***Switch*** | ***Diode*** |
| *Uin*=15 *V* (135 *W*) | 1.88 | 4.19 | 2.63 | 5.2 |
| *Uin*=20 *V* (180 *W*) | 2.19 | 4.64 | 2.58 | 5.36 |
| *Uin*=25 *V* (225 *W*) | 1.75 | 5.036 | 2.65 | 5.52 |
| *Uin*=30 *V* (270 *W*) | 1.64 | 5.36 | 2.61 | 5.67 |
| *Uin*=35 *V* (210 *W*) | 1.25 | 3.81 | 1.88 | 3.89 |

Fig. 8*a* presents theoretical power losses in the semiconductors of the boost and qZS converters in different operation points according to TABLE I. As can be seen, in both converters diode losses increase proportionally to the conduction time but MOSFET losses grow proportionally to the switch *S* duty-cycle or the longer the switch *S* on-state time, the larger are the losses.

Fig. 8*b* shows the theoretical efficiency of both converters neglecting power losses in the inductor, capacitors and PCB tracks.

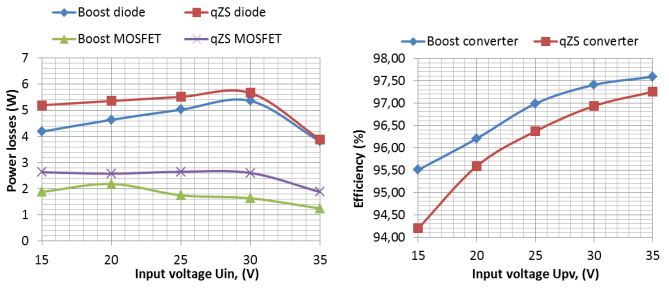


(a) (b)

Fig. 8. Power losses in the diode and the MOSFET of boost and qZS converters in different operation points according to TABLE I.

## IV. Experimental Results

Experiments were made with both of the discussed converters. A general circuit diagram used in our experiments is the same as in Fig. 3. General operation parameters, component types and values are summarized in TABLE II. Both inductors (Fig. 9*b*) in the qZS converter are wound on one core (ETD 29, N87) performing as a coupled inductor [8]. The capacitors of both converters consist of the parallel connection of "Murata" (GRM32ER72A225K) [9].

TABLE II. GENERAL OPERATING PARAMETERS, COMPONENT TYPES AND VALUES

| Operating parameters | Value/type |
|---|---|
| Input voltage, $U_{PV}$ | 15…35 V |
| Intermediate voltage, $U_1$ | 40 V |
| Switching frequency, $f$ | 100 kHz |
| **Components** | |
| Switch, $S$ | Si4190ADY |
| Diode, $V$ | V60D100C |
| Inductors $L_1$=$L_2$ | 22 µH |
| Capacitors $C$=$C_1$=$C_2$ | 26.4 µF |

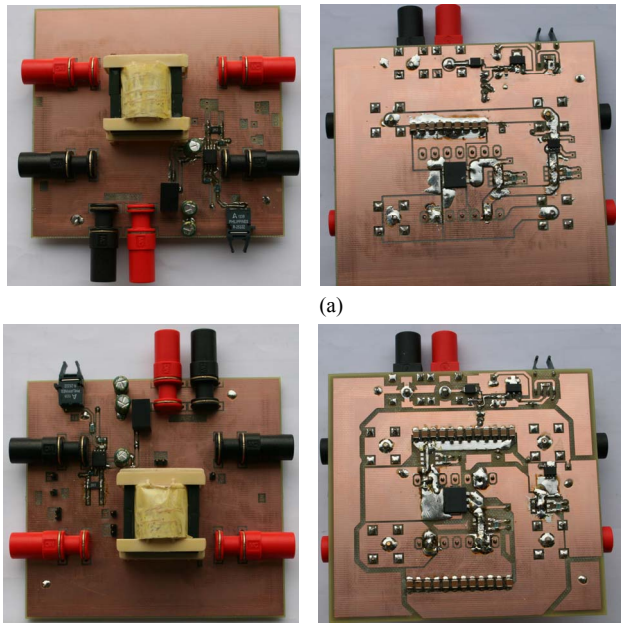

(a)

(b)

Fig. 9. Top and bottom view of both MPPT converter topologies: a) boost converter; b) qZS converter.

Fig. 10 shows the comparison of the theoretical and the experimental efficiency in both of the discussed converters.

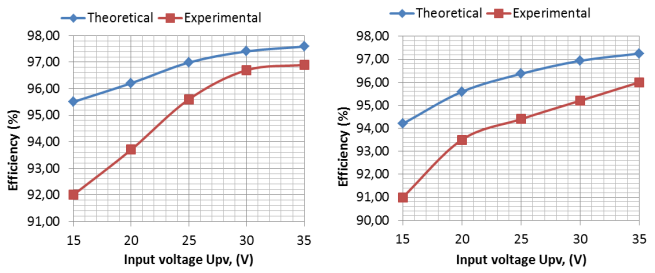


(a) (b)

Fig. 10. Theoretical and experimental efficiency at different operation points: (a) boost converter; b) qZS converter.

Difference between the theoretical and the experimentally obtained efficiency in different operation points is 0.5-3%. As it was expected, the difference between both curves is greater at a higher voltage boost. This difference between the theoretical and the experimental efficiency curves indicates to the components the losses of which were not considered (inductor, capacitors and PCB tracks).

## V. CONCLUSIONS

This paper has presented an analytical and experimental comparative analysis of the boost and qZS topologies as MPPT converters.

Analytical expressions for the estimation of parameters in different operation modes for both of the converters were proposed. Semiconductor loss calculation and estimation were elaborated.

It should be taken into account that the application of the qZS converter needs the turn-off current of the transistor switch to be twice larger than the boost converter, which is the main disadvantage of the qZS converter.

Experimental results show that depending on the input voltage boost (1.2 - 2.7 times), the efficiency of the qZS converter was 91...96% against the boost converter efficiency of 92…97%. It can be concluded that both of the discussed converters show similar results in terms of efficiency. It means that additional features of each converter should be considered when selecting the MPPT converter.

Focus in further studies will be on the analysis of other component losses as well as optimization of the PCB in order to reduce losses in the conductors. Also, synchronous rectification will be considered in order to reduce losses in the diode.

## ACKNOWLEDGMENT

This research work has been supported by Latvian Council of Science (Grant 416/2012).

## REFERENCES

[1] PV stack Saana 245-255 TP3 MBW data sheet http://www.napssystems.com/wordpress/wp-content/uploads/2013/12/DS_SAANA245-255TP3MBW_EN_mail.pdf

[2] Mohan N., Undeland T.,Robbins W. Power Electronic Converters, Application and Design. John Wiley and sons, NY, 1995, 667 p.

[3] Yuan Li; Anderson, J.; Peng, F.Z.; Dichen Liu, "Quasi-Z-Source Inverter for Photovoltaic Power Generation Systems", Twenty-Fourth Annual IEEE Applied Power Electronics Conference and Exposition APEC 2009, pp. 918-924, 15-19 Feb. 2009.

[4] D. Vinnikov, I. Roasto, J. Zakis, R.Strzelecki, "New Step-Up DC/DC Converter for Fuel Cell Powered Distributed Generation Systems: Some Design Guidelines", in journal "Electrical Review" ISSN 0033-2097, Vol. 86, Nr. 8. pp. 245-252, 2010.

[5] J. Zakis, D. Vinnikov, "Study of Simple MPPT Converter Topologies for Grid Integration of Photovoltaic Systems," Scientific Journal of Riga Techical University, Power and Electrical Engineering, 29, 2012, pp 67–72.

[6] Miaosen Shen; Joseph, A.; Jin Wang; Peng, F.Z.; Adams, D.J., "Comparison of Traditional Inverters and Z -Source Inverter for Fuel Cell Vehicles," Power Electronics, IEEE Transactions on , vol.22, no.4, pp.1453,1463, July 20.

[7] D. Graovac, M. Purschel, A. Kiep "MOSFET Power Losses Calculation Using the Data-Sheet Parameters", Infineon Application note, V1.1, July, 2006.

[8] Zakis, J.; Vinnikov, D.; Bisenieks, L. "Some Design Considerations for Coupled Inductors for Integrated Buck-Boost Converters", III International Conference on Power Engineering, Energy and Electrical Drives POWERENG 2011, pp. 1-6, 2011.

[9] J. Zakis, D. Vinnikov, "Implementation Possibilities of SMD Capacitors for High Power Applications," Scientific Journal of Riga Techical University: Power and Electrical Engineering, pp 1 – 6, 2012.



Za is, J., Ra is, I., Ribickis, L. Comparative Analysis of Boost and Quasi-Z-Source Converters as Maximum Power Point Trackers for PV Panel Integrated Converters. In: Proceedings of IEEE 23rd International Symposium on Industrial Electronics (ISIE 2014), Turkey, Istanbul, 1-4 June, 2014. Piscataway, NJ: IEEE, 2014, pp.1991-1995. ISBN 978-1-4799-2399-1. ISSN 2163-5145. Available from: doi:10.1109/ISIE.2014.6864922